

Pressure dependence of the photooxidation of selected carbonyl compounds in air: *n*-butanal and *n*-pentanal

Jovan Tadić^a, Ivan Juranić^{b,*}, Geert K. Moortgat^c

^a Center for Chemistry IChTM, POB 815, Studentski trg 12-16, 11001 Belgrade, Yugoslavia

^b Faculty of Chemistry, University of Belgrade, POB 158, 11001 Belgrade, Yugoslavia

^c Atmospheric Chemistry Department, Max-Planck-Institut für Chemie, POB 3060, 55020 Mainz, Germany

Received 2 April 2001; accepted 10 July 2001

Abstract

Dilute mixtures of *n*-butanal and *n*-pentanal in synthetic air (up to 100 ppm) were photolyzed with fluorescent UV lamps (275–380 nm) in air at 298 K. The main photooxidation products, identified and quantitatively analyzed by FT-IR spectroscopy, were ethene (*n*-butanal) or propene (*n*-pentanal), CO, vinylalcohol and ethanal. The photolysis rates and the absolute quantum yields Φ of both compounds were found to be slightly dependent on the total pressure. At 100 Torr, in the photolysis of *n*-butanal and *n*-pentanal $\Phi_{100} = 0.48 \pm 0.02$ and 0.40 ± 0.04 , whereas at 700 Torr, the total quantum yields were $\Phi_{700} = 0.38 \pm 0.02$ and 0.32 ± 0.01 , respectively. These results could be explained by the collisional deactivation of photoexcited molecules. Two decomposition channels were identified in both cases: the radical channel $RCHO \rightarrow R + HCO$, and the molecular channel $C_xH_yCHO \rightarrow C_{x-1}H_{y-3} + CH_2=CHOH$, having the relative yields of 68 ± 3 and $32 \pm 3\%$ (*n*-butanal), and 20 ± 4 and $80 \pm 4\%$ (*n*-pentanal) at 700 Torr. The product, $CH_2=CHOH$, tautomerizes to ethanal. UV absorption cross-sections were measured prior to photolysis. For the comparison, the products were also analyzed after photolysis of both compounds in teflon bags using direct sunlight. © 2001 Elsevier Science B.V. All rights reserved.

Keywords: Photolysis; Photooxidation; *n*-Butanal; *n*-Pentanal; Quantum yield

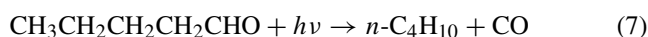
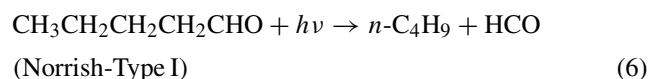
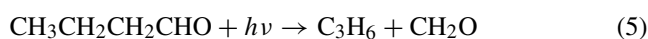
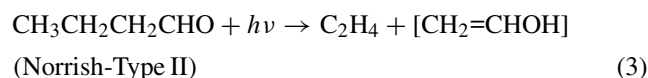
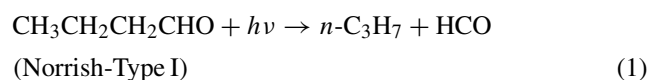
1. Introduction

Aldehydes play a significant role in a variety of atmospheric reactions, such as formation of photochemical smog [1] of peroxyacetyl nitrate (PAN), and of regional ozone. Photo-dissociation of aldehydes represents an important source of free radicals in the lower atmosphere [2–4]. The C_1 – C_5 aldehydes have many sources. They are widely used in industry, and are products of incomplete combustion of petroleum fuels, and of biomass. Smaller alkyl aldehydes are also products of the atmospheric degradation chemistry of hydrocarbons, ethers, alcohols, and other organic compounds. Vegetation, biomass and other living organisms emit many of these compounds.

Many studies have been devoted to the photodissociation of shorter chain aldehydes, such as CH_2O , CH_3CHO , C_2H_5CHO [5–13], and relatively small number have been devoted to longer chain aldehydes, such as C_3H_7CHO and C_4H_9CHO [14–16]. Aliphatic aldehydes exhibit a weak

absorption band in the wavelength range 240–360 nm as a result of a symmetry forbidden $n-\pi^*$ transition [17,18].

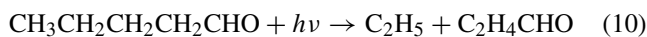
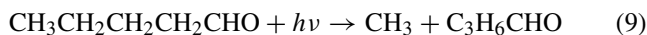
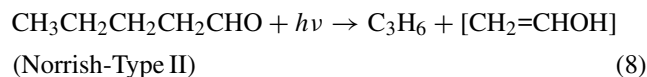
Photolysis of *n*-butanal, and *n*-pentanal could theoretically occur through several ways, where processes (1 and 6) and (3 and 8) are supposed to be of major importance [17].



* Corresponding author.

E-mail addresses: jtadic@eunet.yu (J. Tadić),

ijuranic@chem.bg.ac.yu (I. Juranić).



Processes (1) and (6) are the fragmentations into free radicals, with an enthalpy changes of around 350 kJ/mol corresponding to a photochemical threshold of around 340 nm [15]. The processes (3) and (8), which are common to molecules with a γ -hydrogen atom, are intramolecular rearrangements with enthalpy around 80 kJ/mol ($\lambda \leq 1454$ nm) [15]. The processes (2) and (7) are exothermic, and energetically possible at all applied wavelengths [15]. The enthalpy changes for the processes (3) and (8) were calculated assuming that the keto-form of acetaldehyde is formed in the primary step. As a matter of fact, this assumption is not correct, and, therefore, enthalpy changes of these reactions should be modified for the difference between the heats of formation of enol and keto forms of acetaldehyde.¹ Reactions (4) and (5) were found to be negligible above 280 nm in the photolysis of *n*-butanal [17], and the same assumption for the reactions (9) and (10) seems to be justified.

In this paper, the results obtained from photolysis of *n*-butanal and *n*-pentanal using wide band emission lamps were reported. Absorption cross-sections of these compounds were also measured. We have investigated products and mechanisms of the photooxidation of both alkanals, and measured absolute quantum yields in the pressure range 10–700 Torr. The photooxidation experiments were carried out in a long-path quartz cell with detection of precursors and products by FT-IR spectroscopy. After identification and quantification of the products, a mechanistic description of the photolysis and photooxidation processes was deduced. From the measured decay rate of the starting material, and from the knowledge of the absorption spectrum, overall quantum yields for the photolysis were calculated for various pressures.

2. Experimental

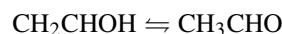
The knowledge of the UV absorption spectra of these two aldehydes was a basic prerequisite for these experiments. They were taken in a fixed path length (63 cm, i.d. 3 cm) thermostated quartz cell (at 25°C) [19,20] and detected by diode array (InstaSpecII, Oriol). A 200 W deuterium lamp (Hereus) and a 60 W tungsten/halogen lamp were used as light sources. After transversing the cell, the light beam was collimated on the entrance slit of a 0.6 mm Czerny–Turner-type monochromator (Jobin–Yvon), where it was dispersed by a grating containing 600 grooves per

millimeter. The spectral resolution of ~ 0.25 nm was determined from the lines of a penray Hg lamp, and was sufficient to resolve any possible peak structure. Absorption cross-sections σ (cm² per molecule) at a given wavelength λ (nm) were derived from the Lambert–Beer's law.

The photooxidation experiments were carried out in a long-path quartz cell with detection of precursors and products by FT-IR spectroscopy. This method provides the possibility of simultaneous detection and monitoring of all the IR-active products and the starting material. The apparatus employed in this work has been described elsewhere [21] and will only briefly be discussed here. The central part of the apparatus is a 44.21 (1.40 m length and 20 cm diameter) quartz cell equipped with two independent sets of White-optic mirror arrangements. Sapphire-coated aluminum mirrors were used in the infrared region ($l = 33.6$ m) for the measurements of the educts and products. A set of MgF₂-coated mirrors was used in the UV–VIS region ($l = 9.82$ m), for measuring the photolysis rates of the actinometer, Cl₂. Infrared spectra at 0.5 cm⁻¹ resolution in the range 450–4000 cm⁻¹ were measured with a Bomem DA8-FT-IR spectrometer. For the UV measurements, the same diode array detector as previously described [22–24] was used.

Photolysis was achieved with six radially mounted lamps, TL12-sunlamps (Philips 40 W TL12 lamps (275–380 nm)). Spectra were taken every 5–10 min with total irradiation time of 30–50 min. The extent of the conversion of the initial compound was approximately 30%. Experiments were carried out at room temperature (298 K), at total pressures between 10 and 700 Torr (1 Torr = (101 325/760) Pa), with initial aldehyde mixing ratios of 100 ppm and more.

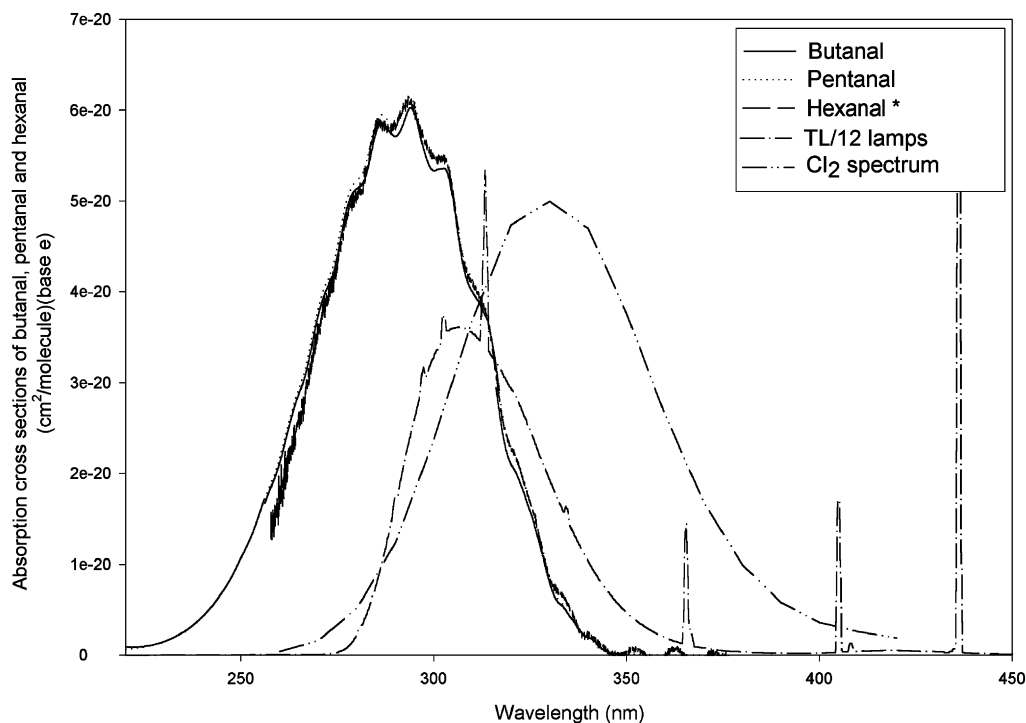
After identification and quantification of the products, a mechanistic description of the photooxidation was deduced, which was tested with the use of the kinetic simulation program FASCIMILE. From the measured decay rate of starting material, overall quantum yields for the photolysis were calculated. Qualitative and quantitative data evaluation was carried out by comparing the products spectra with reference spectra obtained in the same cell, and using calibration curves at corresponding pressures and resolution. The calibration of vinyl alcohol was done indirectly, from the amount of formed ethanal and the simultaneous decrease of the chosen vinyl alcohol peak (peak decrease), since the conversion of these compounds is 1:1 (keto–enol tautomerism) according to:



The concentration of vinyl alcohol determined in this way was used to produce the calibration curve for the selected peak of vinyl alcohol.

The use of a continuous broad band light source allows only the determination of an integral, effective quantum yield Φ^{int} for the photoactive spectral region. Quantum yields were calculated according to the following Eq. (A) [21] (for

¹ The pK value for keto–enol equilibrium is ~ 7 . The corresponding ΔG value is ~ 18 kJ/mol [38].



* Ruppert and Plegens, University of Wuppertal

** Chlorine spectrum is given in arbitrary units

Fig. 1. Emission spectrum of photolysis lamps (TL12/Philips), absorption spectrum of Cl_2 and cross-sections of *n*-butanal, *n*-pentanal and *n*-hexanal [25]. This figure explains why chlorine was used as the actinometer, and why TL12 lamps were chosen for the photolysis, since there is a good overlap of all three regions.

carbonyl compound, C, and actinometer, Act):

$$\Phi^{\text{int}}(\text{C}) = \frac{K_{\text{phot}}(\text{C})}{K_{\text{phot}}(\text{Act}) \left(\frac{\sum \text{OV}(\text{C})}{\sum \text{OV}(\text{Act})} \Phi^{\text{int}}(\text{Act}) \right)} \quad (\text{A})$$

For all TL12-experiments, chlorine was used as actinometer (with $\phi = 1$), using ethane as Cl-atom scavenger. The quantum yield is the single unknown parameter in the equation. The photolysis rates for both compound $K_{\text{phot}}(\text{C})$ and actinometer $K_{\text{phot}}(\text{Act})$ could be directly measured, and the terms $\sum \text{OV}(\text{C})$ and $\sum \text{OV}(\text{Act})$ represent the calculated overlap of lamp emission and absorption spectrum of substrate. The emission spectrum of TL12 lamp along with the cross-sections of *n*-butanal, *n*-pentanal and *n*-hexanal [25] and the absorption chlorine spectrum are shown in Fig. 1.

Several experiments were performed in a teflon bag using sunlight as photolysis source with a longer exposure time of ~3 h. In this case, the ratio CO/ethene or CO/propene was used to determine the importance of Norrish-Type I and II channels, for *n*-butanal and *n*-pentanal, respectively.

Carbonyl compounds were obtained from Sigma-Aldrich Company with 99% purity for *n*-butanal and 97% for *n*-pentanal. Before use, all samples were degassed by several freeze-pump-thaw cycles. Compound purity was checked

by FT-IR spectral measurements and no impurities were found.

3. Results and discussion

3.1. UV absorption cross-sections

The UV spectra of *n*-butanal and *n*-pentanal are displayed in Fig. 2 along with literature [15,26] results. The final 298 K absorption cross-sections reported in Table 1 is based on the average derived from 5–10 experiments. They are averaged over 1 nm interval. Considering both random and systematic errors (pressure and path length), the overall uncertainty in our cross-section measurements is less than 5%.

Our absorption cross-sections for *n*-butanal are in excellent agreement with those previously measured by Martinez et al. [26], the difference at the maximum being less than 3%. However, our values for *n*-pentanal are about 5–20% smaller (~8% at the maximum) than those obtained by Cronin and Zhu [15], as shown in Fig. 2. If the latter values would be correct, they would not represent the observed trend, that all similar aldehydes display almost the same UV absorption cross-sections, both in shape and in intensity [26], as can be seen in Fig. 1 for *n*-butanal, *n*-pentanal and *n*-hexanal. Such

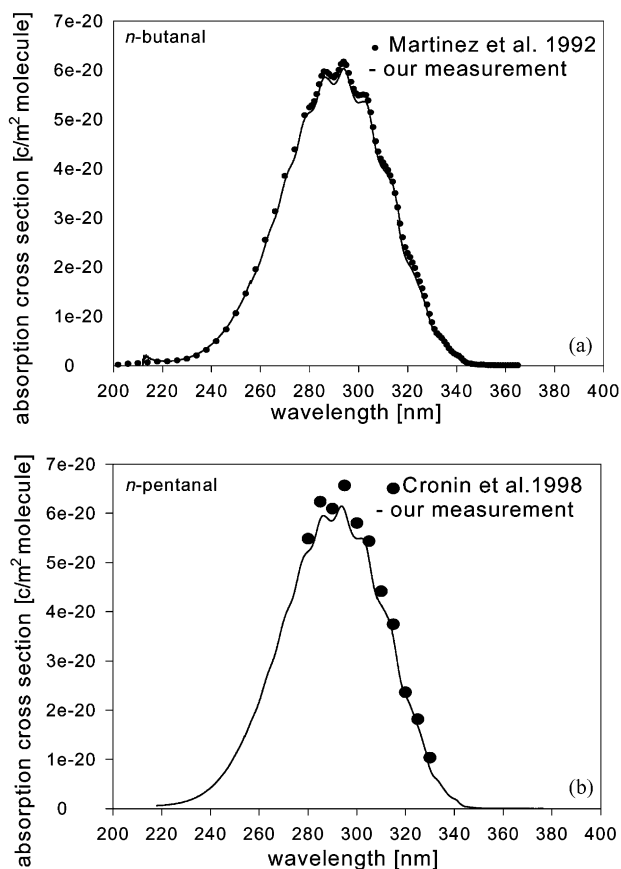


Fig. 2. Absorption cross-sections of *n*-pentanal (a); *n*-butanal (b); and *n*-pentanal [15] and *n*-butanal [26] cross-sections previously measured (for numerical data see Table 1).

behavior can be explained by the relative independence of the UV absorbing carbonyl group on the existence of methyl groups at the end of the chain. Because of that, our results are probably more reliable.

3.2. Photolysis of *n*-butanal

Fig. 3 shows common FT-IR spectrum of an irradiated mixture of *n*-butanal and synthetic air, before and after the photolysis. The displayed spectra are corrected for the background absorption of the pure synthetic air. Major products of the *n*-butanal photolysis in air were found to be CO (multiplet, $2037\text{--}2235\text{ cm}^{-1}$), ethene (949.5 cm^{-1}), enol form of ethanal ($1078, 1118, 1260\text{ cm}^{-1}$), ethanal ($1348.5\text{--}1355.5\text{ cm}^{-1}$) and CO_2 ($2290\text{--}2384\text{ cm}^{-1}$).

Based on the observed products, the mechanism can be confined on both Norrish-Type I and II processes:



Reaction (1) generates two radicals that immediately react with oxygen, to produce peroxy radicals. The HCO radical quantitatively reacts with oxygen, giving CO and HO_2

Table 1

Cross-sections of *n*-butanal and *n*-pentanal

Wavelength (nm)	Absorption cross-section (cm^2 per molecule)	
	<i>n</i> -Butanal	<i>n</i> -Pentanal
230.00	1.53E-21	1.47E-21
231.00	1.69E-21	1.63E-21
232.00	1.88E-21	1.81E-21
233.00	2.08E-21	2.01E-21
234.00	2.32E-21	2.24E-21
235.00	2.56E-21	2.48E-21
236.00	2.84E-21	2.76E-21
237.00	3.16E-21	3.08E-21
238.00	3.51E-21	3.42E-21
239.00	3.87E-21	3.80E-21
240.00	4.28E-21	4.20E-21
241.00	4.72E-21	4.65E-21
242.00	5.22E-21	5.14E-21
243.00	5.75E-21	5.69E-21
244.00	6.34E-21	6.27E-21
245.00	6.94E-21	6.88E-21
246.00	7.56E-21	7.52E-21
247.00	8.26E-21	8.23E-21
248.00	9.05E-21	9.03E-21
249.00	9.91E-21	9.90E-21
250.00	10.80E-21	10.80E-21
251.00	11.70E-21	11.70E-21
252.00	12.60E-21	12.60E-21
253.00	13.60E-21	13.60E-21
254.00	14.70E-21	14.70E-21
255.00	16.00E-21	15.70E-21
256.00	17.10E-21	17.00E-21
257.00	17.80E-21	18.20E-21
258.00	18.90E-21	19.30E-21
259.00	20.00E-21	20.40E-21
260.00	21.30E-21	21.80E-21
261.00	22.90E-21	23.40E-21
262.00	24.60E-21	25.10E-21
263.00	26.20E-21	26.70E-21
264.00	27.60E-21	28.10E-21
265.00	28.80E-21	29.30E-21
266.00	30.10E-21	30.60E-21
267.00	31.60E-21	32.30E-21
268.00	33.50E-21	34.30E-21
269.00	35.60E-21	36.40E-21
270.00	37.50E-21	38.20E-21
271.00	39.00E-21	39.70E-21
272.00	40.20E-21	40.80E-21
273.00	41.10E-21	41.90E-21
274.00	42.30E-21	43.30E-21
275.00	44.20E-21	45.20E-21
276.00	46.40E-21	47.50E-21
277.00	48.60E-21	49.50E-21
278.00	50.10E-21	50.90E-21
279.00	51.00E-21	51.80E-21
280.00	51.40E-21	52.20E-21
281.00	51.70E-21	52.80E-21
282.00	52.50E-21	53.70E-21
283.00	54.00E-21	55.30E-21
284.00	55.90E-21	57.30E-21
285.00	57.60E-21	58.80E-21
286.00	58.50E-21	59.50E-21
287.00	58.40E-21	59.40E-21
288.00	58.00E-21	59.00E-21
289.00	57.40E-21	58.50E-21
290.00	57.10E-21	58.50E-21

Table 1 (Continued)

Wavelength (nm)	Absorption cross-section (cm ² per molecule)	
	<i>n</i> -Butanal	<i>n</i> -Pentanal
291.00	57.60E-21	59.10E-21
292.00	58.50E-21	60.10E-21
293.00	59.80E-21	61.20E-21
294.00	60.30E-21	61.40E-21
295.00	59.60E-21	60.60E-21
296.00	58.10E-21	59.00E-21
297.00	56.20E-21	57.20E-21
298.00	54.70E-21	55.90E-21
299.00	53.70E-21	55.10E-21
300.00	53.40E-21	54.90E-21
301.00	53.50E-21	54.90E-21
302.00	53.60E-21	54.90E-21
303.00	53.50E-21	54.60E-21
304.00	52.30E-21	53.10E-21
305.00	49.90E-21	50.60E-21
306.00	46.90E-21	47.60E-21
307.00	44.10E-21	45.00E-21
308.00	42.10E-21	43.10E-21
309.00	40.80E-21	42.10E-21
310.00	40.00E-21	41.30E-21
311.00	39.30E-21	40.50E-21
312.00	38.60E-21	39.50E-21
313.00	37.60E-21	38.40E-21
314.00	36.70E-21	36.90E-21
315.00	34.60E-21	34.60E-21
316.00	32.10E-21	31.70E-21
317.00	25.60E-21	28.50E-21
318.00	24.00E-21	25.80E-21
319.00	22.20E-21	24.00E-21
320.00	21.00E-21	22.90E-21
321.00	20.20E-21	21.90E-21
322.00	19.30E-21	20.80E-21
323.00	18.20E-21	19.50E-21
324.00	16.90E-21	18.10E-21
325.00	15.70E-21	16.70E-21
326.00	14.40E-21	15.30E-21
327.00	12.90E-21	13.70E-21
328.00	11.20E-21	12.00E-21
329.00	9.44E-21	10.90E-21
330.00	7.90E-21	8.01E-21
331.00	6.68E-21	6.89E-21
332.00	5.93E-21	6.28E-21
333.00	5.55E-21	5.82E-21
334.00	5.09E-21	5.16E-21
335.00	4.45E-21	4.44E-21
336.00	3.84E-21	3.74E-21
337.00	3.19E-21	3.08E-21
338.00	2.63E-21	2.55E-21
339.00	2.23E-21	2.20E-21
340.00	1.96E-21	1.97E-21
341.00	1.78E-21	1.67E-21
342.00	1.42E-21	1.14E-21
343.00	0.91E-21	0.73E-21
344.00	0.57E-21	0.48E-21
345.00	0.39E-21	0.35E-21
346.00	0.26E-21	0.28E-21
347.00	0.20E-21	0.23E-21
348.00	0.12E-21	0.20E-21
349.00	0.03E-21	0.17E-21
350.00	0.01E-21	0.15E-21

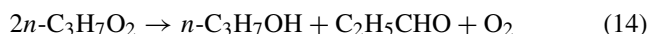
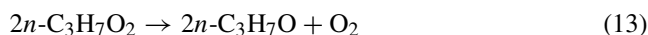
[5,27,28], allowing the usage of primary formed CO as the indicator for process (1)



n-Propyl radicals also react with oxygen, forming *n*-propylperoxy radicals



The fate of *n*-propylperoxy radicals is to react with itself, and/or to disproportionate, or to react with HO₂, to produce a variety of products [29].

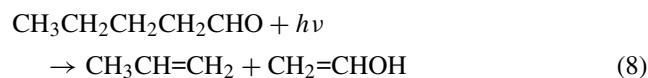
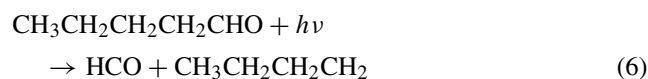


The reactions (13) and (14) between peroxy radicals are very slow [30], so that it is to be expected that the *n*-propylperoxy radicals will dominantly react with HO₂, formed in reaction (11), via reaction (16). The amounts of expected products from these reactions were below the detection limit of the applied analytical method (less than 1 mTorr). Also, no evidence was found for the presence of the products of other possible channels.

Since ethene is a stable molecular species at the applied conditions, it was used as the indicator for the molecular process (3).

3.3. Photolysis of *n*-pentanal

The photolysis of *n*-pentanal was performed in the same manner as for *n*-butanal. Propene (910–914 cm⁻¹) was detected as a product of the Norrish-Type II decomposition process, instead of ethene in the case of *n*-butanal.



The products of the Norrish-Type I decomposition were CO (formed in the reaction of primary produced HCO radical with oxygen, reaction (11)), and the *n*-butyl radical, which will react with oxygen to form the *n*-butylperoxy radical. Here, also, the products of reactions of *n*-butylperoxy radical were either below the detection limit, or their peaks interfered with the peaks of initial compound (see analogue reaction paths in photolysis of *n*-butanal).

Time profiles of all product concentrations in *n*-pentanal photolysis of one typical experiment are shown in Fig. 4. All concentrations are represented by partial pressures (mTorr),

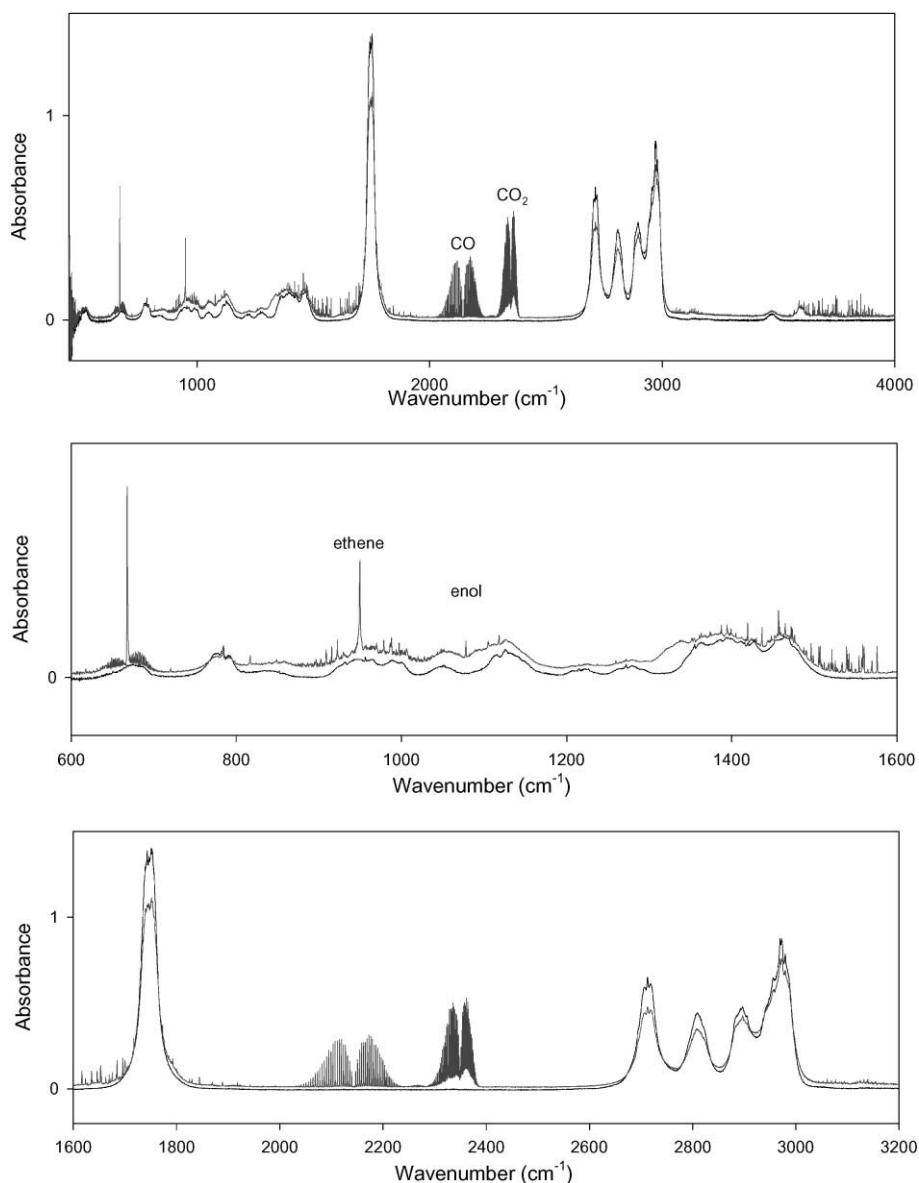


Fig. 3. FT-IR spectrum of 100 mTorr *n*-butanol, before (black) and after photolysis (gray) (six TL12 lamps, 100 Torr synthetic air). Major products CO, ethene and ethanol, and CO₂ as a by-product, are marked (exact positions of the peaks are given in the text).

except for vinyl-alcohol, which is represented by the time profile of its peak integral given in arbitrary units. Fig. 5 displayed relative yields of products ($\Delta_{\text{products}}/(-\Delta_{\text{pentanal}})$). From the concentration profiles of the products, it could be deduced, which products are formed primarily, and which products are also involved in secondary reactions. From Fig. 5, it could be seen that propene is a primary product, stable at the applied conditions. The sum of vinyl alcohol and ethanal concentrations is constant, and is equal to the concentration of propene. Vinyl alcohol itself is involved in secondary conversion reaction to ethanal. Corollary, ethanal is a secondary product. Carbon monoxide is both primary and secondary product. The CO₂ is considered as an artifact, originating from desorption of organic material from the wall of the reactor.

3.4. Yields of Norrish-Type I and II processes

The results could be interpreted in two different ways. First, as the relative probability for the photoexcited molecule to undergo Norrish-Type I or II decomposition. Second, as absolute yield of the Norrish-Type I and II processes, deduced from the ratio of the process indicator molecule (primary CO and propene or ethene) to the amount of educt consumed (*n*-butanal or *n*-pentanal; see Fig. 5). The absolute quantum yield of the Norrish-Type I or II processes is, additionally, a function of the total absolute quantum yield and is, therefore, dependent on the total pressure.

The relative probability for *n*-butanal molecule to undergo different decomposition channels is shown in Table 2. The probabilities for both *n*-butanal and *n*-pentanal

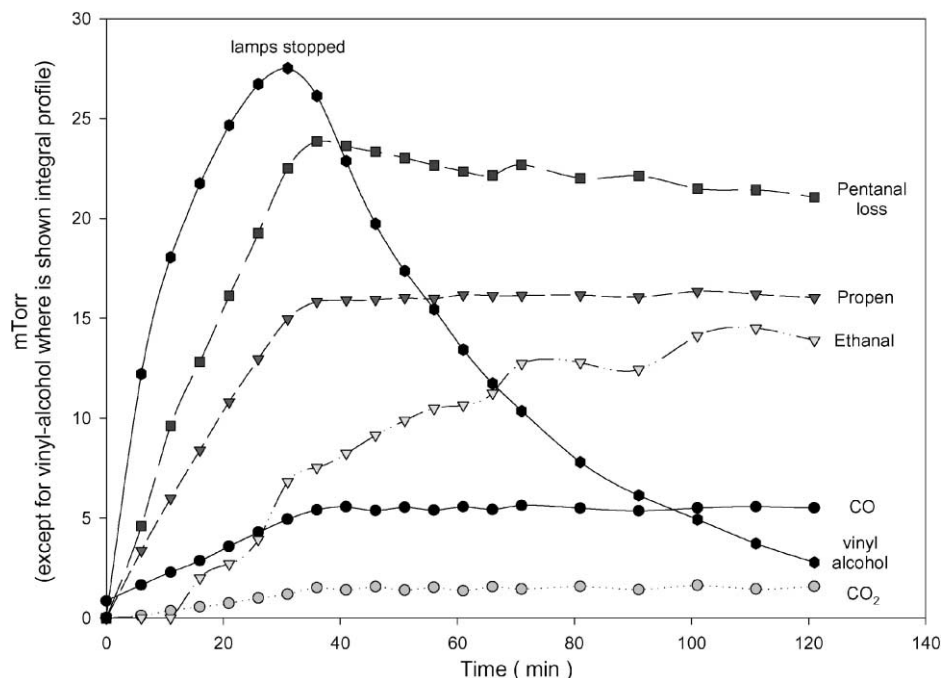


Fig. 4. Photolysis of *n*-pentanal: the products formation vs. loss in *n*-pentanal. The curve of CO shows that CO is not only the primary reaction product, but also a product of the subsequent reactions. Ethanal is the secondary product. See comments on Fig. 5.

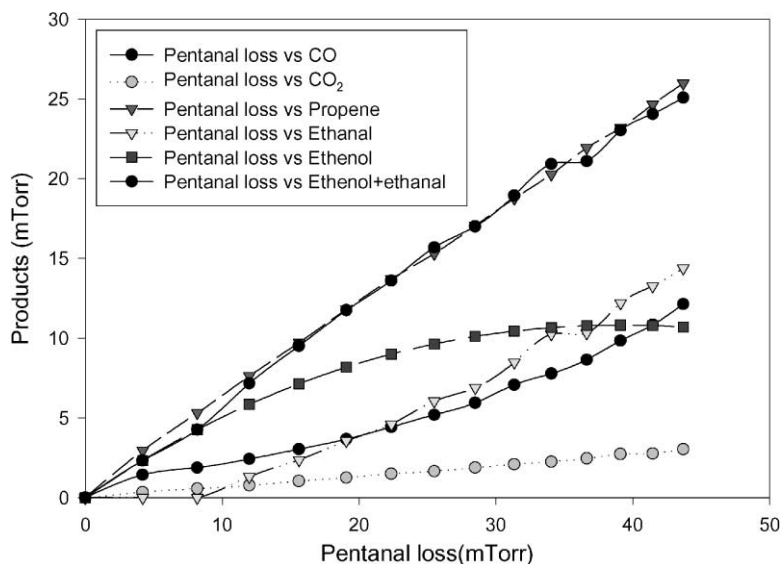


Fig. 5. Photolysis of *n*-pentanal: time profile–variation of the concentrations of products. Ethanol partial pressure reaches maximum and then starts to decrease by conversion to ethanal.

Table 2

Relative probabilities for *n*-butanal and *n*-pentanal molecule to undergo different decomposition channels, TL12 lamps (errors represent the experimental scatter)

	Norrish-Type I	Norrish-Type II
<i>n</i> -Butanal	68 ± 3%	32 ± 3%
<i>n</i> -Pentanal	20 ± 4%	80 ± 4%

are deduced from the ratio of primary formed CO, and of ethene and propene, respectively. The Norrish-Type I process is the dominant decomposition channel for *n*-butanal (68 ± 3%). In contrast, the probabilities of the different decomposition channels for *n*-pentanal molecule after light absorption are opposite to those of *n*-butanal. For *n*-pentanal the Norrish-Type II fragmentation represents the main decomposition channel (80 ± 4%). The relative importance of

Table 3

Relative probabilities for *n*-butanal and *n*-pentanal molecule to undergo Norrish-Type I and/or II decomposition channels, by direct sunlight irradiation (errors represent the experimental scatter)

	Norrish-Type I	Norrish-Type II
<i>n</i> -Butanal	79 ± 1%	21 ± 1%
<i>n</i> -Pentanal	30 ± 2%	70 ± 2%

the molecular channel increases with chain length, changing from 32 ± 3% for *n*-butanal to 80 ± 4% for pentanal, but then remains nearly constant higher alkanals: 73% was measured for *n*-hexanal [31], and about 80% for *n*-heptanal [32].

Results obtained using direct sunlight are reported in Table 3, and the same trend is observed as in the experiments done in the laboratory. These measurements were not time-resolved, but based on end-products analysis, and this introduces an uncertainty in the determination of the primary formed CO as the indicator of the Norrish-Type I process, since the determination requires the knowledge of the process dynamics, not only of the final value. The numbers shown in Table 3 were obtained assuming that 30% of the observed CO upon the photolysis with direct sunlight has an origin in secondary reactions. This is justified since a non-linear increase of the CO yield was observed in laboratory experiments (see Fig. 5).

Table 4 represents the absolute yields values for primary formed CO and ethene or propene divided by the loss of initial aldehyde. These values, multiplied with the total quantum yield value at the desired pressure, give the quantum yield values for both Norrish-Type I and II processes. The carbon balance for the experiments with *n*-butanal is close to unity (90–95%). In the case of *n*-pentanal, the carbon balance shows values significantly lower than unity (0.64 ± 0.09).

Table 4

Absolute yields of Norrish-Type I and II decomposition products for *n*-butanal and *n*-pentanal photolysis (errors represent the experimental scatter)

Total pressure (Torr)	<i>n</i> -Butanal		<i>n</i> -Pentanal	
	Norrish-Type I ($\Delta_{\text{product CO}}/\Delta_{\text{butanal}}$)	Norrish-Type II ($\Delta_{\text{propene}}/\Delta_{\text{butanal}}$)	Norrish-Type I ($\Delta_{\text{product CO}}/\Delta_{\text{pentanal}}$)	Norrish-Type II ($\Delta_{\text{propene}}/\Delta_{\text{pentanal}}$)
100	65.43	31.82	13.98	55.19
100	68.96	31.32	12.16	50.38
100	59.35	29.55	8.40	42.09
100	63.22	31.20	14.35	50.50
300	65.75	30.06	13.99	52.43
300	64.66	29.82	14.86	46.98
300	63.40	29.49	11.11	51.03
500	58.46	28.30	12.53	60.35
500	64.33	27.98	8.16	47.97
500	62.15	27.93	–	–
700	57.54	26.70	12.03	53.31
700	58.23	26.89	17.71	59.51
700	58.85	30.48	–	–
Average	62.3 ± 6.6	29.3 ± 2.5	12.7 ± 5.0	51.8 ± 9.6

3.5. Absolute quantum yields

One of the objectives of the study was to determine the absolute quantum yield dependency of studied molecules on the total pressure. Chlorine was applied as the actinometer. From the decay of *n*-butanal and *n*-pentanal, the photolysis rate constants were deduced for the different pressures by plotting the natural logarithm of concentration versus time (first-order decay), and performing a regression analysis. From these results, overall quantum yields were calculated according to the Eq. (A) using the overlap integrals of *n*-butanal and *n*-pentanal/TL12, and of Cl₂/TL12, and the experimentally determined photolysis rate of actinometer.

For both aldehydes, the absolute quantum yield displayed a dependency on total pressure. The values for absolute quantum yields at different total pressures are given in Table 5. These values relate to the extent of absolute quantum yields of Norrish-Type I and II decomposition channels. Fig. 6 summarizes the total quantum yield data displayed as a Stern–Volmer plot, where the reciprocal quantum yield is plotted against the total pressure *P*. The total quantum yield Φ is calculated from the following equations: $1/\Phi = 1.81 + (1.931 \times 10^{-3})P$ (*n*-butanal), and $1/\Phi = 2.44 + (7.771 \times 10^{-4})P$ (*n*-pentanal). The slopes of the regression lines correspond to the sensitivities of absolute quantum yields on the total pressure *P*. Recent quantum yield data obtained for *n*-hexanal [31] are also included in Fig. 6.

Earlier studies by Blacet and Calvert [33] determined quantum yield in the photolysis of 100 Torr pure *n*-butanal at 313 nm of 0.50 for CO and 0.18 for C₂H₄, giving a total yield for both Norrish processes of 0.68. These authors argue that ethylene uniquely originates from reaction channel (3), whereas CO is formed from the dissociation of the HCO radical (channel 1) into CO and H atoms, which undergo further secondary reactions, abstracting H atoms from

Table 5
Absolute quantum yield values for *n*-butanal, *n*-pentanal and *n*-hexanal at different pressures of synthetic air, TL12 lamps (errors represent the experimental scatter)

Total pressure (Torr)	<i>n</i> -Butanal	<i>n</i> -Pentanal	<i>n</i> -Hexanal ^a
10	0.61	–	–
10	0.58	–	–
	0.59 ± 0.02	–	–
50	0.53	–	–
50	0.52	–	–
50	0.51	–	–
	0.52 ± 0.01	–	–
100	0.47	–	–
100	0.50	0.40	0.43
100	0.47	0.44	0.41
100	0.47	0.36	0.44
	0.48 ± 0.02	0.40 ± 0.04	0.43 ± 0.02
300	0.43	0.37	0.41
300	0.44	0.39	0.42
300	0.44	0.36	0.43
	0.44 ± 0.01	0.38 ± 0.02	0.42 ± 0.01
500	0.30	0.36	0.43
500	0.37	0.36	0.38
500	0.37	0.33	0.41
	0.35 ± 0.05	0.35 ± 0.02	0.40 ± 0.03
700	0.32	0.35	0.40
700	0.33	0.34	0.37
700	0.32	0.33	0.37
	0.32 ± 0.01	0.34 ± 0.01	0.38 ± 0.02

^a [31].

n-butanal, whereby CO is further produced. Obviously the observed CO quantum yield is too large. These data can be compared to our broad band photolysis quantum yield data at 100 Torr of 0.48 (see Table 5). At atmospheric conditions, (760 Torr) the total quantum yield for the dissociation processes is 0.31 for *n*-butanal and 0.33 for *n*-pentanal.

Since the intercept at zero pressure is not equal to 1 (the intercepts are 1.81 and 2.44), as should be expected if collisional deactivation is the only relaxation process besides the photodecomposition, it seems evidently that there are other energy-dissipating processes. Possibly, the triplet state of *n*-butanal and *n*-pentanal could deactivate by phosphorescence etc. [34]. The interaction with the walls deactivating to the ground state is probably of minor importance because of large volume-to-surface ratio.

Recently Cronin and Zhu [15] performed photolysis experiments on *n*-pentanal, using dye laser photolysis followed by cavity ring down spectroscopy for direct monitoring of the HCO radicals. The primary yield of HCO radical (0.06 up to 0.20) was determined directly at selected wavelengths in the range 280–325 nm. Fig. 7 shows their values in comparison with our data extrapolated at zero pressure. It is surprising that no total pressure dependency (in the range 8–480 Torr pure nitrogen) was observed, while our measurements show that there is a slight pressure dependency in photolysis studies performed in air. To be able to compare their data obtained at selected wavelengths with our measurement using wide band emission lamp, their data were averaged over the 280–380 nm region, in order to maintain the same quantum yield/wavelength overlap. The only assumption that had to be made is the value at 340 nm, which is also the threshold for the Norrish-Type I

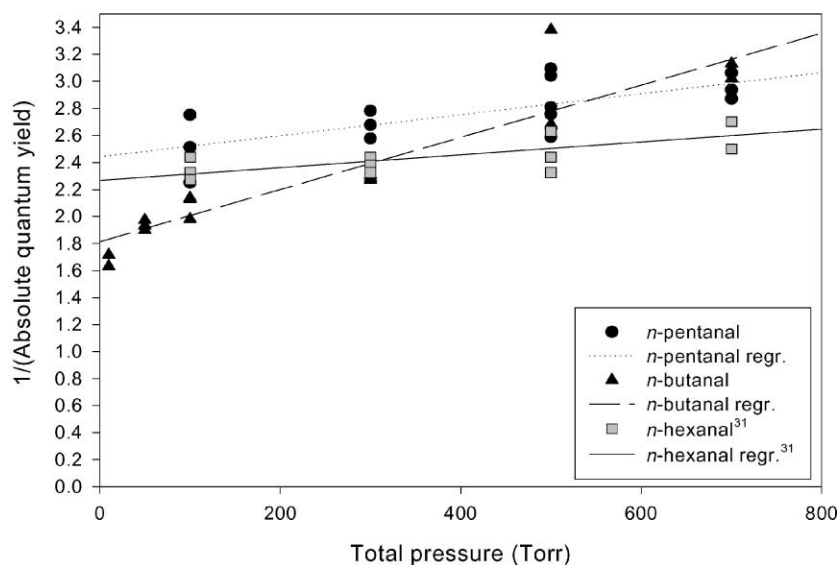


Fig. 6. Pressure dependency of 1/(absolute quantum yield) in *n*-butanal and *n*-pentanal photolysis, at different total pressures of synthetic air (Stern–Volmer plot).

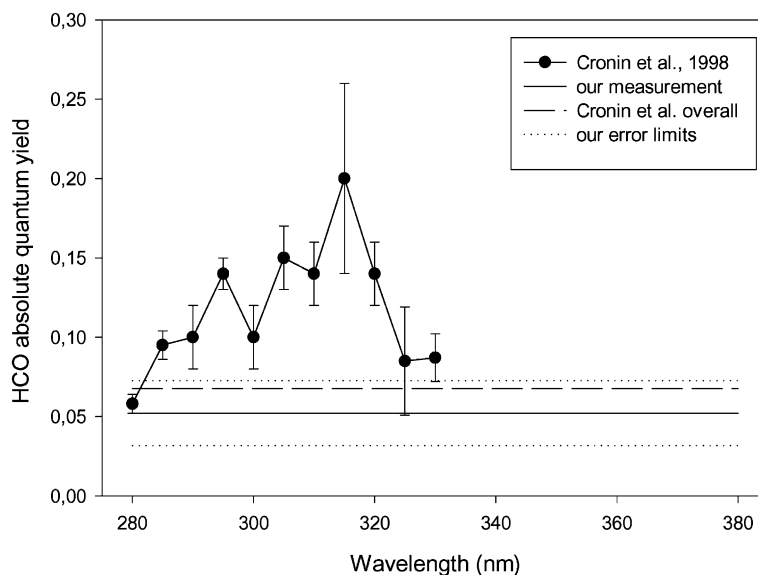


Fig. 7. The HCO absolute quantum yields; our measurement and literature data [15].

process. The assumed value was 0.052, which is the average value for the whole region obtained at zero pressure in our measurements. Their integral value for the quantum yield over the 280–380 nm range amounts to 0.0676, whereas an average quantum yield of 0.052 was obtained in this study.

3.6. Other possible processes

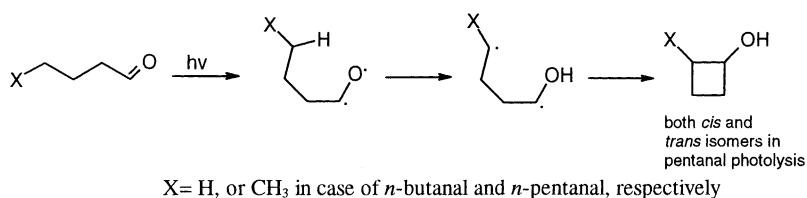
The reactions (1–10) are all energetically possible at the applied part of the UV spectra but actually only Norrish-Type I and II processes were observed. The carbon balance values lower than unity indicate that there may be other decomposition channel than Norrish-Type I or II. The detection of the products of photocyclization of the photoexcited *n*-pentanal molecules was done recently (Scheme 1) [35]. According to the suggested mechanism, photoexcited *n*-pentanal molecules undergo photocyclization, forming *cis/trans* isomers of 2-ethyl-cyclobutanol.

There is also a theoretical possibility for *n*-butanal molecules to undergo photocyclization, forming cyclobutanol following the same manner (Scheme 1). However, these cyclo compounds were not detected in our experiments.

3.7. Atmospheric implications

It is well established that the main degradation processes of carbonyl compounds are controlled by photolysis and by the reaction with OH radicals. The atmospheric lifetime of both alkanals can be estimated from the knowledge of the OH reaction rate constants and the photodissociation rates. The rate constant for the OH + *n*-butanal was estimated as $k_{\text{OH,b}} = 2.35 \times 10^{-11}$ cm³ per molecule per second, based on the studies by Semmes et al. [36] (2.27×10^{-11} cm³ per molecule per second) and Kerr and Sheppard [37] (2.4×10^{-11} cm³ per molecule per second). For *n*-pentanal the recently measured value of $k_{\text{OH,p}} = 2.7 \times 10^{-11}$ cm³ per molecule per second was used [35]. Taken an average noon-time OH concentration of 2×10^6 molecule cm⁻³, the reactive lifetime for *n*-butanal $\tau_{\text{OH,b}} = 5.9$ h and $\tau_{\text{OH,p}} = 5.1$ h for *n*-pentanal.

Maximum daytime photolysis rates were estimated during in situ measurements in the photochemical outdoor reactor [35], as $k_{\text{ph,b}} = (1.0 \pm 0.2) \times 10^{-5}$ s⁻¹ for *n*-butanal and $k_{\text{ph,p}} = (1.6 \pm 0.15) \times 10^{-5}$ s⁻¹ for *n*-pentanal, corresponding to a photolytic lifetime of 28 and 17 h, respectively. This would indicate that the dominant removal process for these aldehydes in the lower troposphere is the reaction with OH



Scheme 1.

radicals, but that photolytic processes still take some part in the degradation.

Since photolysis leads to the formation of additional radicals, they have enormous importance with regard to the atmospheric oxidation capacity, and local formation of ozone and other photooxidants. In view of the results obtained in this study, combined with the absolute quantum yields and branching ratios for radical formation (Tables 4 and 5), the absolute radical yield at atmospheric conditions can be estimated for *n*-butanal as $62.3 \times 0.32 = 20\%$, and $12.7 \times 0.34 = 4.3\%$ for *n*-pentanal. If quantum yields for aldehydic compounds values are not known (e.g. for the use in atmospheric modeling), it is common to assume that they are unity, which is seldom the case as shown in this study. This leads to an overestimation of the calculated radicals produced by photolysis processes.

References

- [1] R. Atkinson, *Atmos. Environ.* A24 (1990) 1.
- [2] T.E. Graedel, L.A. Farrow, T.A. Weber, *Atmos. Environ.* 10 (1976) 1095.
- [3] D. Grosjean, *Environ. Sci. Technol.* 16 (1982) 254.
- [4] B.J. Finlayson-Pitts, J.N. Pitts, Jr., *Atmospheric Chemistry*, Wiley, New York, 1986.
- [5] G.K. Moortgat, W. Seiler, P. Warneck, *J. Chem. Phys.* 78 (1983) 1185.
- [6] Y. Carmely, A. Horowitz, *Int. J. Chem. Kinet.* 16 (1984) 1585.
- [7] C.B. Moore, J.C. Weishaar, *Ann. Rev. Phys. Chem.* 34 (1983) 525.
- [8] P. Ho, D.J. Bamford, R.J. Buss, Y.T. Lee, C.B. Moore, *J. Chem. Phys.* 76 (1982) 3630.
- [9] A. Horowitz, J.G. Calvert, *J. Phys. Chem.* 86 (1982) 3105.
- [10] H. Meyrahn, G.K. Moortgat, P. Warneck, in: *Proceedings of the 15th Informal Conference on Photochemistry*, Stanford, CA, July 1982.
- [11] P.B. Shepson, J. Heicklen, *J. Photochem.* 19 (1982) 215.
- [12] J. Heicklen, J. Desai, A. Bahta, C. Harper, R. Simonaitis, *J. Photochem.* 34 (1986) 117.
- [13] A.C. Terentis, P.T. Knepp, S.H. Kable, *J. Phys. Chem.* 99 (1995) 12704.
- [14] S. Forgetter, T. Berces, S. Dobe, *Int. J. Chem. Kinet.* 11 (1979) 219.
- [15] J.T. Cronin, L. Zhu, *J. Phys. Chem.* 102 (1998) 10274.
- [16] L. Zhu, J.T. Cronin, A. Narang, *J. Phys. Chem. A* 103 (1999) 7248.
- [17] J.G. Calvert, J.N. Pitts, Jr., *Photochemistry*, Wiley, New York, 1966, p. 369, 373–374.
- [18] E.K.C. Lee, R.S. Lewis, *Adv. Photochem.* 12 (1980) 1.
- [19] R. Meller, W. Raber, J.N. Crowley, M. Jenkin, G.K. Moortgat, *J. Photochem.* A62 (1991) 163.
- [20] A. Nolle, H. Heydtmann, R. Meller, W. Schneider, G.K. Moortgat, *Geophys. Res. Lett.* 19 (1992) 281.
- [21] G.K. Moortgat, R.A. Cox, G. Schuster, J.P. Burrows, G.S. Tyndall, *J. Chem. Soc., Faraday Trans. II* 85 (1989) 809.
- [22] W.H. Raber, G.K. Moortgat, *Advance series in physics and chemistry (Part 3)*, in: J.R. Barker (Ed.), *Progress and Problems in Atmospheric Chemistry*, World Scientific Publishing Co., Singapore, 1995, p. 318.
- [23] J.N. Crowley, G.K. Moortgat, *J. Chem. Soc., Faraday Trans.* 88 (1992) 2437.
- [24] R. Meller, W. Raber, J.N. Crowley, M. Jenkin, G.K. Moortgat, *J. Photochem.* A62 (1991) 163.
- [25] H. Plagens, R. Bröske, M. Splitter, L. Ruppert, I. Barnes, K.H. Becker, in: *Proceedings of the Second Workshop of the Eurotrac-2 Sub-project CMD, Chemical Mechanism Development*, 23–25 September 1998, Karlsruhe.
- [26] R.D. Martinez, A.A. Buitrago, N.W. Howell, C.H. Hearn, J.A. Joens, *Atmos. Environ.* 26 (1992) 785.
- [27] A. Horowitz, J.G. Calvert, *Int. J. Chem. Kinet.* 10 (1978) 805.
- [28] A. Horowitz, F. Su, J.G. Calvert, *Int. J. Chem. Kinet.* 10 (1978) 1099.
- [29] R. Atkinson, *J. Phys. Chem. Ref. Data, Monograph* 2 (1994).
- [30] P.D. Lightfoot, R.A. Cox, J.N. Crowley, M. Destriau, G.D. Hayman, M.E. Jenkin, G.K. Moortgat, F. Zabel, *Atmos. Environ. (special issue)* 26A (1992) 1805.
- [31] J. Tadić, I. Juranic, G.K. Moortgat, *Molecules* 6 (2001) 287.
- [32] J. Tadić, I. Juranic, G.K. Moortgat, submitted for publication.
- [33] F.E. Blacet, J.G. Calvert, *J. Am. Chem. Soc.* 73 (1954) 661.
- [34] R.P. Borkowski, P. Ausloos, *J. Am. Chem. Soc.* 84 (1962) 4044.
- [35] G.K. Moortgat, Final report on EU project RADICAL: evaluation of radical sources in atmospheric chemistry through chamber and laboratory studies ENV4-CT97-0419, March 2000.
- [36] D.H. Semmes, H.R. Ravishankara, C.A. Gump-Perkins, P.H. Wine, *Int. J. Chem. Kinet.* 17 (1985) 303.
- [37] J.A. Kerr, D.W. Sheppard, *Environ. Sci. Technol.* 15 (1981) 960.
- [38] R.P. Bell, P.W. Smith, *J. Chem. Soc. B*, 241, 1966.